Lithos 340–341 (2019) 108–123

Contents lists available at ScienceDirect

Lithos

journal homepage: www.elsevier.com/locate/lithos

A comparison between phase diagram modelling of metamafic rocks and experimental and independent thermobarometric data

Caio Arthur Santos [a,*], Renato Moraes [b], Gergely A.J. Szabó [b]

[a] Institute of Geosciences - University of São Paulo, Rua do Lago, 562, 05508-080 São Paulo (SP), Brazil
[b] Department of Mineralogy and Geotectonics, Institute of Geosciences - University of São Paulo, Rua do Lago, 562, 05508-080, São Paulo (SP), Brazil

ARTICLE INFO

Article history:
Received 27 November 2018
Accepted 27 April 2019
Available online 04 May 2019

Keywords:
Mafic rocks
Pseudosections
THERMOCALC

ABSTRACT

The use of equilibrium phase diagrams such as pseudosections has become widespread in recent years, but few studies tested the phase relations predicted by these models. This work aims at comparing predicted phase relations with mineral assemblages observed in experimental products and in natural samples, in this latter case using as reference metamorphic conditions pressures and temperatures determined for metapelites metamorphosed under the same conditions as the mafic rocks. Pseudosections were calculated with THERMOCALC for six mafic bulk-rock compositions, in the range 425–700 °C and 2–8 kbar. The resulting diagrams can be divided into two groups: one in which a classic sequence of mineral assemblages occur and another where quartz is unstable and diopside is stable throughout. The results compare well to the independent data in three of the six studied cases. The main inconsistencies found in the pseudosections are underestimation of the stability field of garnet and overestimation of the stability fields of diopside and hornblende, which is at odds not only with data specific to the rocks studied here, but with the literature on metamafic rocks in general. In the case of garnet, the most likely case of discrepancy is the absence of Mn in the activity-composition models available. On the other hand, the issue with diopside and hornblende is much harder to evaluate, as it may be related to any of the activity-composition models, or to relationships between two or more of them. Nonetheless, we can affirm that the overestimation of the diopside stability field is related to SiO_2 content, although there are other factors that influence it.

1. Introduction

Mineral assemblage stability diagrams, widely known as pseudosections, are phase diagrams calculated for a specific bulk-rock composition, or range of compositions. In relation to *P-T* projections, or petrogenetic grids, they have the advantage of only presenting equilibria relevant to this given composition or range of compositions, which makes pseudosections much easier to read and interpret. The use of this kind of diagram has become widespread in Metamorphic Petrology since the 1990s (Connolly and Petrini, 2002; Lanari and Duesterhoeft, 2019; Powell and Holland, 2008; Yakymchuk et al., 2017).

Despite the intense calculation of these diagrams, there are relatively few papers that specifically aim at testing thermodynamic modelling results (*e. g.*Grant, 2009; Tibaldi et al., 2011; White et al., 2011, Forshaw et al., 2019) although there are several papers that combine it with other methods (*e.g.*Korhonen et al., 2014; Lanari et al., 2013; Tual et al., 2018).

In the present work, the approach is to compare modelled phase relationships with experimental results and assemblages observed in natural rocks. In the latter case, we adopt as reference conditions the pressures and temperatures determined on metapelites that were metamorphosed under the same conditions as the mafic rocks we studied. Comparison with experiments has an evident value, as *P* and *T* are controlled. However, there may be problems, as experiments may not produce equilibrium assemblages, and analysis of the products can be problematic (see White et al., 2011, for a specific discussion on this subject). The *P-T* estimates we adopt as reference data for the natural rocks have, as any *P-T* estimates, limitations of their own, but we trust that, keeping these limitations in mind, the comparison can be helpful to the community.

By comparing thermodynamic modelling results with data from other rock types we are, in principle, testing the approach as whole, *i.e.* the software, thermodynamic descriptions of phases and the activity-composition models, since the results depend on it all. However, by now the methods implemented in THERMOCALC (and in other software such as Perple_X and Theriak-Domino) are, after decades of application, well established (Connolly and Petrini, 2002; de Capitani and Brown, 1987; Powell et al., 1998, 2005; Powell and Holland, 2008) in a way that, if there are problems, they are much more likely to stem from the thermodynamic data. Of these, the activity-composition models are the most poorly constrained, as their accuracy cannot be directly measured. So, in a work such as the present one, we are evaluating the activity-composition models and, to a lesser degree, the thermodynamic data.

* Corresponding author.
E-mail address: caio.santos@usp.br (C.A. Santos).

https://doi.org/10.1016/j.lithos.2019.04.024
0024-4937/

Table 1
Chemical composition of the studied samples. All values given in weight %. FeO values with a "*" are total Fe.

Sample	IZ 006	RM 201	SM 495	RM 29e	AL, 83	Sp, 81
SiO_2	54.22	45.81	46.85	51.06	50.44	49.43
TiO_2	0.85	2.23	1.40	2.97	1.79	1.62
Al_2O_3	18.16	13.66	14.92	10.39	13.37	15.97
FeO	8.04*	12.82	12.07*	13.78	11.93*	9.43*
Fe_2O_3		2.76		2.14		
MnO	8.51	0.21	0.20	0.22	0.21	0.18
MgO	3.31	6.55	7.63	5.43	6.58	8.50
CaO	0.70	10.26	11.55	8.69	10.95	10.73
Na_2O	0.19	3.43	2.51	2.28	3.76	2.87
K_2O	8.51	0.62	0.21	0.42	0.19	0.18
P_2O_5	3.31	0.18	0.13	0.25	0.20	0.15
Total	97.81	98.53	97.47	97.63	99.42	99.06

2. Materials and methods

2.1. Sample choices

Six mafic compositions were selected for modelling (Table 1 and Fig. 1): two amphibolites from the Juscelândia Sequence, Goiás, Brazil, (Moraes et al., 2003; Moraes and Fuck, 1999), one amphibolite from the Votuverava Group, São Paulo, Brazil (Campanha et al., 2015; Faleiros et al., 2011), one amphibolite from the Ivrea Zone, Northern Italy (Kunz et al., 2014) and the compositions utilized in the experimental works of Spear (1981) and Apted and Liou (1983). The criteria for selecting the samples were the possibility of performing the kind of analysis we intended, what means availability of published bulk-rock composition and experimental/thermobarometric data to which the modelled phase equlibria could be compared. Additionally, we had access to samples of two of the case studies (the samples from Votuverava Group and Juscelândia Sequence). In these cases thin sections were analyzed with a petrographic microscope, while for the others the descriptions were taken from the literature along with the compositions.

2.2. Thermodynamic modelling

P-T pseudosections covering the range 425–700 °C and 2–8 kbar were calculated for all compositions using version 3.45 of THERMOCALC (Powell and Holland, 1988), and dataset ds62 (Holland and Powell, 2011, created February 6th, 2012). The activity-composition models used (including phases that were available but did not appear in the calculations) were as follows: amphibole, clinopyroxene and tonalitic melt from Green et al. (2016); garnet, orthopyroxene, biotite, muscovite and chlorite from White et al. (2014a); olivine and

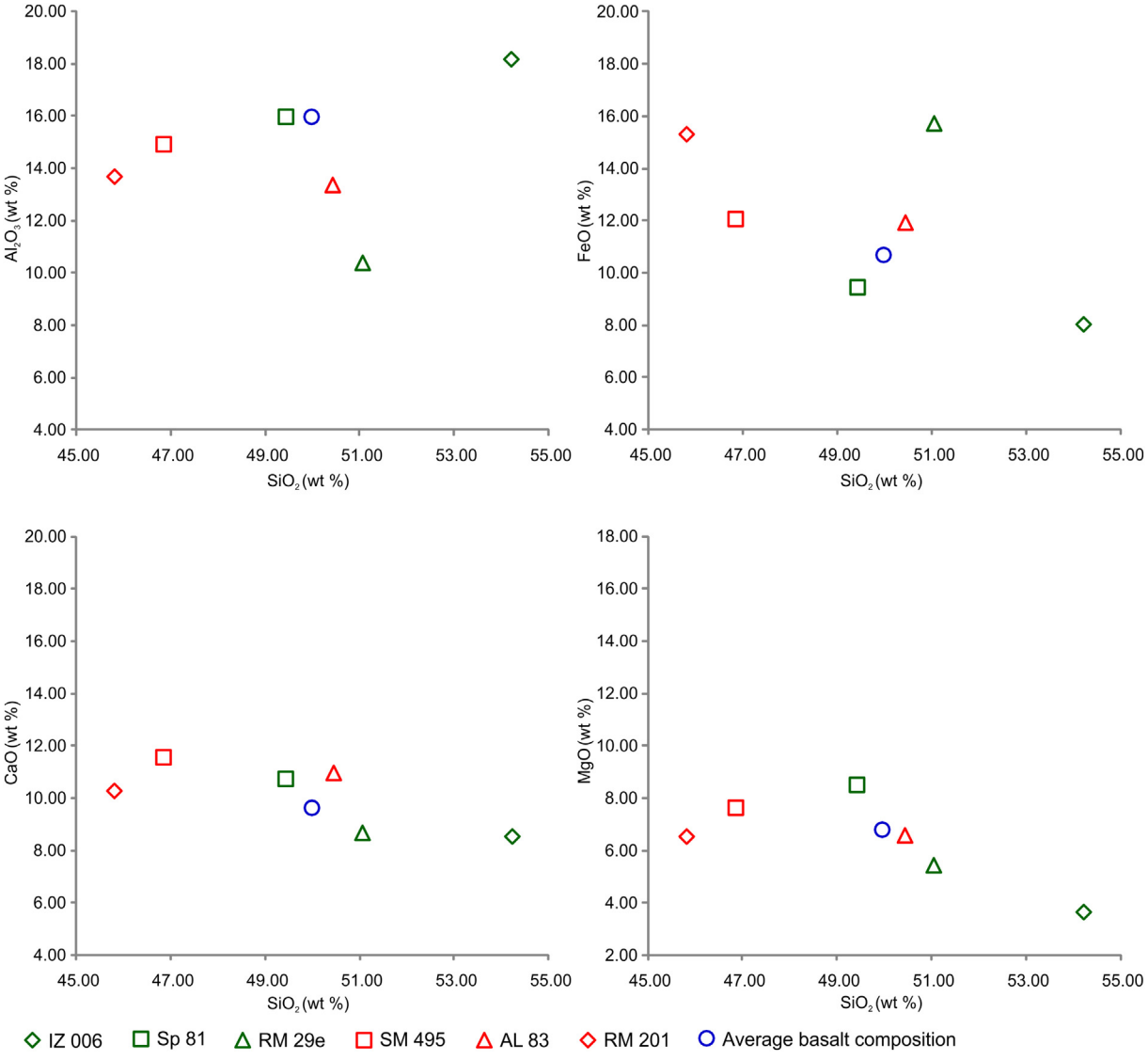

Fig. 1. Bivariate plots comparing the chemical composition of the studied samples. Also plotted is the average basalt composition according to Le Maitre (1976).

Table 2
The actual, mol % chemical compositions used in the calculations with THERMOCALC. In the cases where FeO and Fe_2O_3 have been reported separately, Fe was recalculated to be all FeO, as THERMOCALC handles X_{Fe3+} by adding an O component (see Diener and Powell, 2010) whose assumed value for each sample is given in this table. The O entry for sample AL 83 shows two values because two pseudosections (with different X_{Fe3+} values) were calculated.

Sample	IZ 006	RM 201	SM 495	RM 29e	AL, 83	Sp, 81
SiO_2	59.70	49.2	50.2	55.00	53.30	51.90
TiO_2	0.70	1.80	1.10	2.40	1.40	1.30
Al_2O_3	11.80	8.60	9.40	6.60	8.30	9.90
FeO	7.40	13.70	10.80	14.20	10.50	8.30
MgO	6.00	10.50	12.20	8.70	10.40	13.30
CaO	10.00	11.70	13.20	9.90	12.20	12.00
Na_2O	3.50	3.60	2.60	2.40	3.90	2.90
K_2O	0.50	0.40	0.10	0.30	0.10	0.10
O	0.74	1.10	1.10	0.80	0.60/1.21*	0.50

epidote from Holland and Powell (2011); feldspars from Holland and Powell (2003); spinel (which includes magnetite) from White et al. (2002) and ilmenite and hematite from White et al. (2000). Quartz, albite, sphene and rutile were considered as pure phases.

Green et al. (2016) present two clinopyroxene activity-composition models: the "omphacite model", that takes into account order-disorder in M1 and M2 sites, thus allowing high pressure omphacite and jadeite compositions to be calculated, including coexistence between a phase rich in these end-members and diopside; and the "augite model", that does not consider order-disorder in M1 and M2 sites but allows Al into T site and Fe^{2+} and Mg into M2 site, thus allowing high temperature augite and pigeonite compositions to be calculated. At the *P-T* range covered here, the two models produce similar results (Green et al., 2016), what is confirmed by tests performed in this work (not shown). Since for some compositions modelled here omphacite is calculated to be stable at parts of the covered *P-T* spectrum (see below), the "omphacite model" was used in all calculations.

2.3. Bulk-rock compositions

The bulk-rock compositions taken from literature were converted to oxide mol% in order to be used with THERMOCALC (Table 2). The chemical model system used is NCKFMASHTO, with Mn being ignored. All P_2O_5 was considered to be stored on apatite, and the equivalent amount of CaO was removed from each composition. This assumption seems reasonable, as apatite was present in the three samples that could be analyzed petrographically, and no other phosphate was detected. Similarly, Kunz et al. (2014) cite apatite as one of the accessories present in the group of samples IZ 006 belongs to, and does not mention any other phosphate. No apatite is mentioned in the run products of Spear (1981) and Apted and Liou (1983), but neither are other phosphates, so, given its common occurrence in mafic rocks of these metamorphic conditions, apatite is assumed to be the P_2O_5-bearing phase.

Fluid is considered to be in excess in all calculations, and the fluid is considered to be pure H_2O. Since this will generally lead to unrealistic melt proportions (*e.g.* Droop and Brodie, 2012; Weinberg and Hasalová, 2015), no melt bearing equilibria were calculated, except for the *solidus* curve.

Regarding the $Fe^{3+}/(Fe^{3+}+Fe^{2+})$ ratio, therefore denoted as X_{Fe3+}, the compositions used in experiments and the compositions intended to be compared to natural samples represent different situations: experiments, as discussed by Diener and Powell (2010), are carried out under controlled f_{O2}, while in nature this is unlikely. Following the cited authors, in the case of pseudosections intended to be compared to experimental work, the chemical potential of oxygen, μ_O, was calculated simultaneously with the phase diagram results, *via* calcmuo script, and the values obtained were compared to the *P-T-*μ_O diagrams for buffering assemblages presented by Diener and Powell (2010), in order to define the X_{Fe3+} value that should be used. Obviously, since the calculated μ_O varies along the covered *P-T* range, this is not an exact approach, but it remains a reasonable approximation.

On the other hand, the compositions intended to be compared to data from natural rocks pose the same challenge faced by regular studies using pseudosections, since reliable X_{Fe3+} data is much harder to obtain than regular bulk-rock an mineral chemistry data (Diener and Powell, 2010; White et al., 2000). For two of the compositions used only total Fe was reported. In these cases X_{Fe3+} was set to 0.2, close to the mean value given for MORBs by Lecuyer and Ricard (1999), and, additionally, the effects of varying the ratio were investigated using *P-*X_{Fe3+} pseudosections covering values of X_{Fe3+} between 0.0 and 0.3. For the other two samples bulk-rock Fe_2O_3 contents were reported. As discussed by Diener and Powell (2010) bulk-rock analysis are likely to overestimate (to some unknown extent) the Fe^{3+} content, due to weathering and to oxidation during sample preparation. As these analysis returned X_{Fe3+} values already below those used for the other two samples, the values were only rounded down to 0.12 and 0.16.

3. General features of pseudosections for mafic compositions

The calculated pseudosections can be divided in two groups: the first includes samples IZ 006, RM 29e and the sample used in the experimental work of Spear (1981), which will therefore be referred to as "Sp 81" (Figs. 2a-b, 3a). Diagrams calculated for this group display sequences of mineral assemblages compatible with the classic metamorphic facies (Apted and Liou, 1983; Bucher and Grapes, 2011; Laird, 1980). They resemble the pseudosections presented by Diener et al. (2007), Diener and Powell (2012) and Green et al. (2016): greenschist facies conditions are characterized by the mineral assemblage actinolite + epidote + chlorite + albite + sphene + quartz + biotite and, as temperature rises, actinolite, chlorite, albite and epidote are consumed, while hornblende and plagioclase become stable, followed by diopside at middle amphibolite facies (Figs. 2a-b, 3a). Under low pressure conditions plagioclase can be predicted to be stable at lower temperatures than hornblende, and chlorite and actinolite persist to temperatures higher than those reached by epidote, while at higher pressure the reverse occurs. Albite is predicted to be consumed shortly after plagioclase appearance, except for sample Sp 81 at low pressures, where epidote is removed and albite is calculated to persist for some tens of °C after plagioclase appearance. Low pressure and high temperature conditions favor ilmenite over sphene. Quartz is present throughout, except for temperatures higher than 590 °C and pressures lower than 3 kbar in sample Sp 81 (Fig. 2b). Garnet only appears at $P > 11$ kbar (see below) and glaucophane appears at low temperature, and pressure higher than 7 kbar in the pseudosection calculated for sample RM29e (Fig. 3a).

The second group includes the remaining samples: The composition used in the experimental work of Apted and Liou (1983), which will therefore be referred to as "AL 83" and samples RM 201 and SM495. The main differences between this group and the previous one are the predicted stability fields of diopside and quartz, with the first being present and the second being absent from greenschist facies conditions through most of the covered *P-T* spectrum (Figs. 3b, 4a-b). Other differences include hornblende being stable at lower temperatures than in the first group, and that the onset of blueschist facies mineral assemblages is marked by the appearance of omphacite, rather than glaucophane. The behavior of other minerals, such as actinolite, chlorite and epidote, is similar to what is observed for bulk compositions of the first group.

Quartz and diopside behave very similarly in the pseudosections calculated for these samples: diopside can be modally important in greenschist facies (up to 20%), then quickly decreases after hornblende appearance (its proportion actually goes to zero for two compositions) and then increases gradually with *T* increase, with a quick increase after ilmenite starts to replace sphene as the Ti-bearing phase. Quartz appears at 450–500 °C and is usually not stable below 3–4 kbar. In a *T-x* pseudosection between compositions of samples belonging to

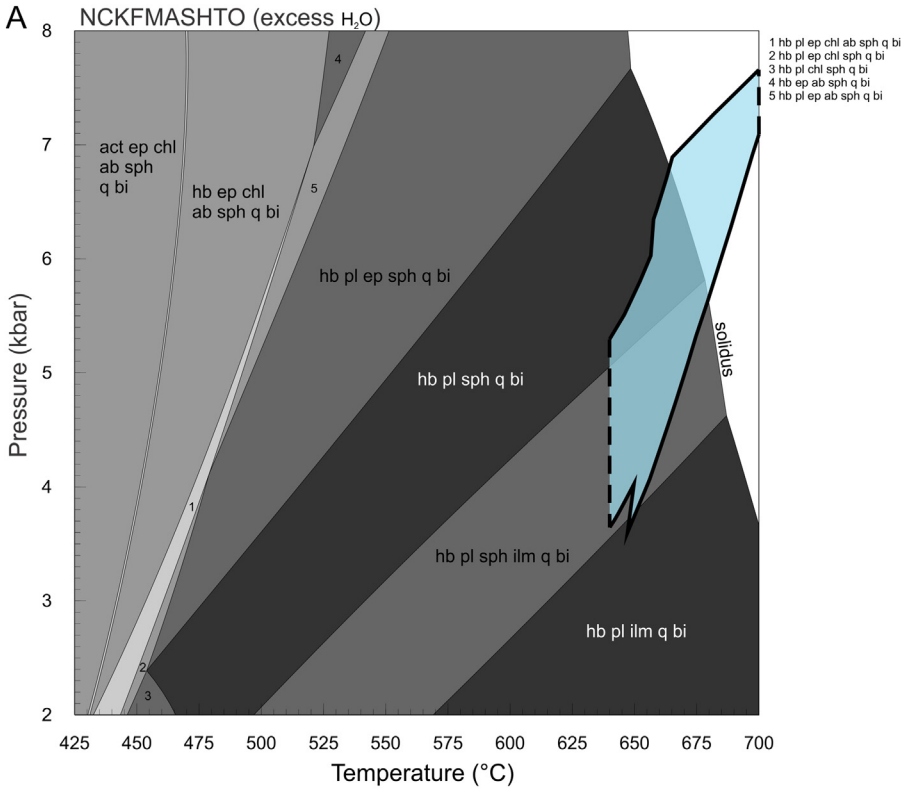

Sample IZ 006 from Kunz *et al.* (2014). $Fe^{3+}/(Fe^{3+}+Fe^{2+}) = 0.2$.

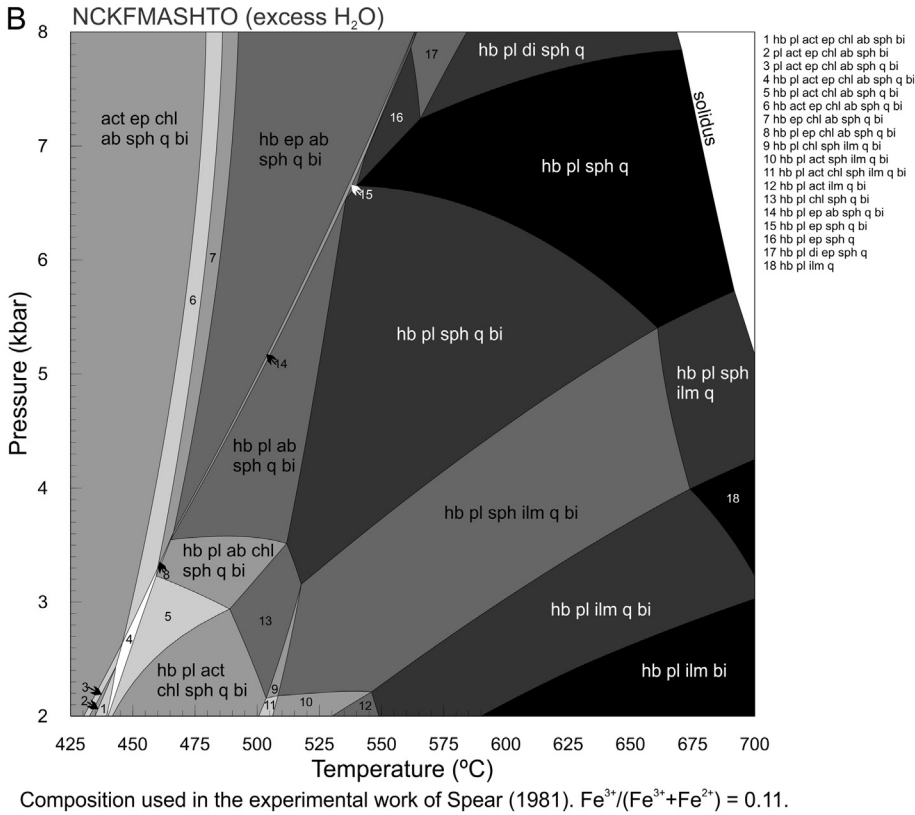

Composition used in the experimental work of Spear (1981). $Fe^{3+}/(Fe^{3+}+Fe^{2+}) = 0.11$.

Fig. 2. (a) *P-T* pseudosection calculated for sample IZ 006. The blue field represents the *P-T* field delimited by Redler et al. (2012) for a metapelite associated to the rock studied here. The dashed borders sign that this field extends to temperatures lower than the low *T* limit of Redler et al.'s (2012) pseudosection and higher than the high-*T* limit of the pseudosection calculated here. All mineral abbreviations follow Holland and Powell (2011) (b) *P-T* pseudosection calculated for sample Sp 81. (For interpretation of the references to colour in this figure legend, the reader is referred to the web version of this article.)

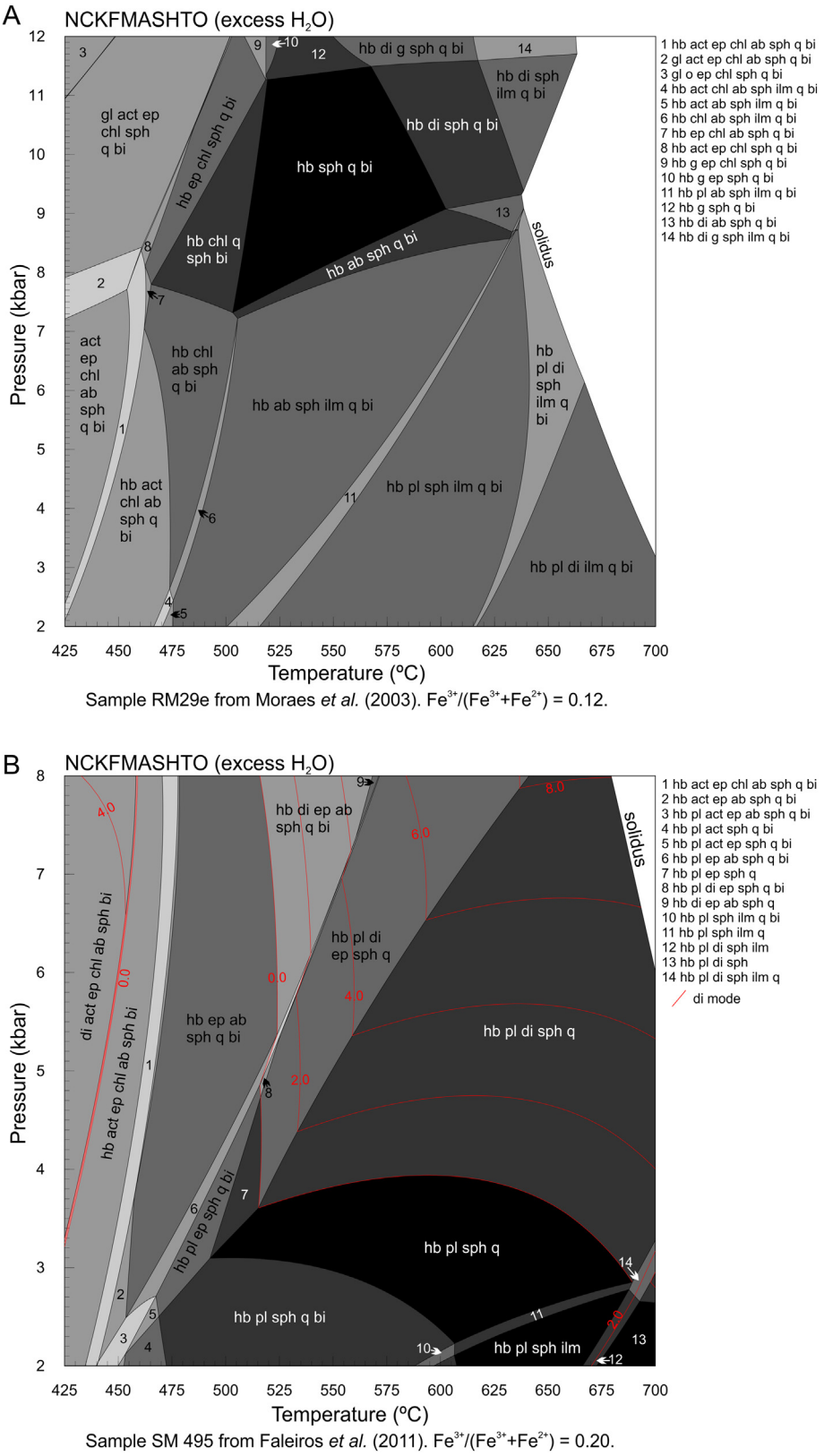

Fig. 3. *P-T* pseudosections calculated for samples RM 29e (a) and SM 495 (b).

each group (Fig. 5) it can be shown that the two characteristics (absence of quartz and presence of diopside) are linked: along the compositional traverse, diopside appears shortly after quartz runs out. In fact it can be noted in the *P-T* pseudosections that compositions that display the highest diopside modes are the ones with the smaller quartz stability fields. Furthermore a pattern such what is predicted for SM 495, where diopside runs out after hornblende appearance and returns to the assemblage at temperatures 80–100 °C higher, is reproduced by a composition in the middle of the Sp 81-AL83 traverse, like x = 0.7, for example.

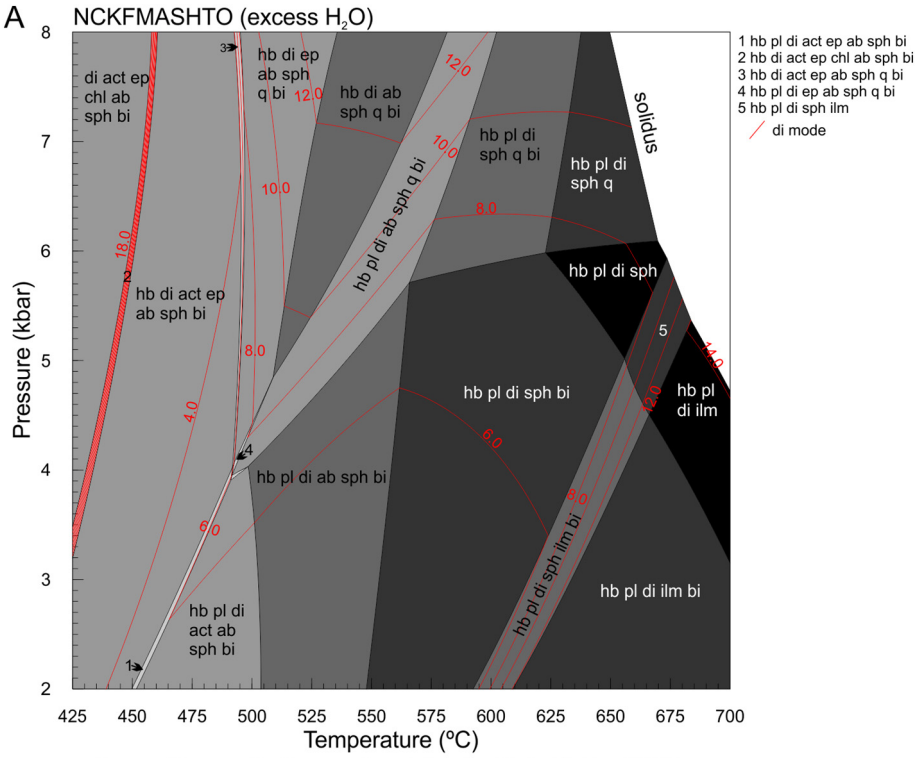

Composition used in the experimental work of Apted & Liou (1983).
$Fe^{3+}/(Fe^{3+}+Fe^{2+})$ = 0,11.

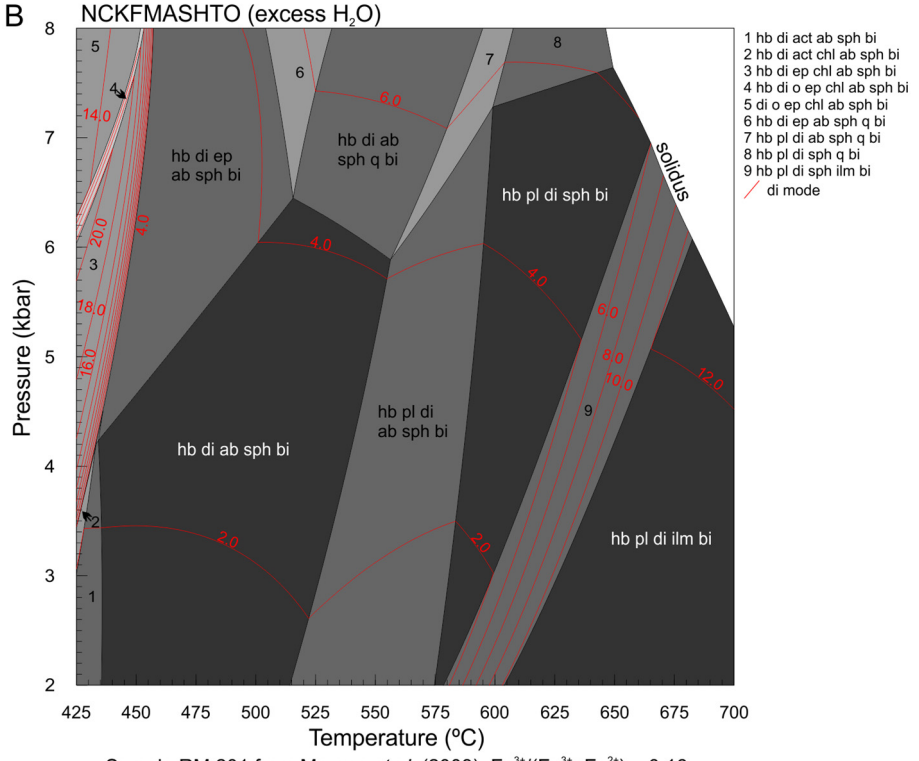

Sample RM 201 from Moraes *et al.* (2003). $Fe^{3+}/(Fe^{3+}+Fe^{2+})$ = 0.16

Fig. 4. *P-T* pseudosections calculated for sample AL 83 (a) and RM 201 (b).

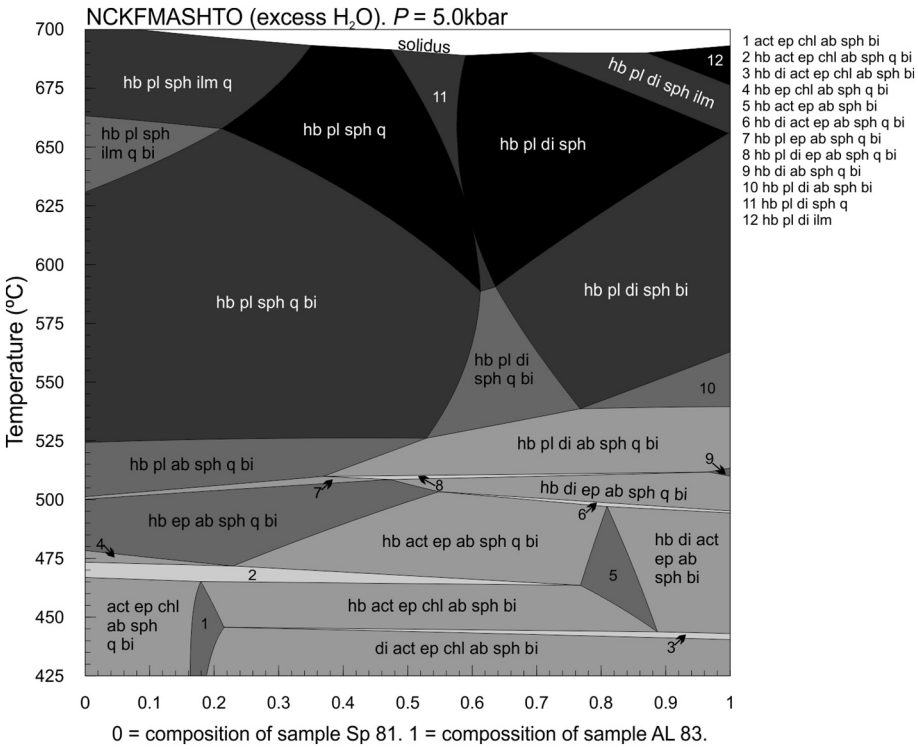

Fig. 5. *T-x* pseudosection calculated between the compositions of the samples Sp 81 and AL 83, showing the transition between "normal" mineral assemblages and diopside-bearing assemblages. $P = 5.0$ kbar.

4. Comparison between modelled and observed mineral assemblages

4.1. Sample IZ 006

This sample is an amphibolite from the Ivrea Zone (northern Italy), whose description and composition were taken from Kunz et al. (2014). There are numerous works on all aspects of the geology of this region (*e.g.* Schmid et al., 1987; Henk et al., 1997; Handy et al., 1999; Luvizotto and Zack, 2009; Sinigoi et al., 2011; Redler et al., 2012, among many others). As reference conditions we adopt the results obtained by Redler et al. (2012), who studied a metapelite (sample IZ 010) from the same unit as sample IZ 006, and geographically close to it, as seen in the maps presented by the two works (Fig. 5 from Redler et al., 2012 and Fig. 2 from Kunz et al., 2014). Redler et al. (2012) calculated pseudosections and refined the *P-T* results using the mineral modes. Specifically for sample IZ 010, they obtained a field extending from <650 °C to ≈ 710 °C and from ≈ 3.4 to ≈ 8 kbar (Fig. 2a, see also their Fig. 10).

IZ 006 is a weakly foliated amphibolite composed of hornblende, plagioclase, quartz, biotite and ilmenite. In the pseudosection, this assemblage is predicted to be stable at a rather large field, which stretches from 590 °C to >700 °C, and from <2 kbar to just over 4.5 kbar (Fig. 2a). The temperatures calculated for the metapelites and the metamafic rocks are in good agreement, but the pressures inferred by modelling the mafic composition are lower, so that the stability fields actually superimpose only in a tiny area of the diagram at approximately 650 °C and 4.7 kbar.

Fig. 6 is a P-X_{Fe3+} pseudosection calculated at 655 °C and between $X_{Fe3+} = 0.0$ and $X_{Fe3+} = 0.3$. It shows that, reducing X_{Fe3+} has the general effect of shifting phase boundaries up pressure. The P range of the metapelite stability field, for $T = 655$ °C, is superimposed on the pseudosection, and it can be seen that for slightly lower X_{Fe3+} values, there is good agreement between the conditions inferred by modelling the mafic composition and the reference conditions.

4.2. Sample Sp 81

The sample used by Spear (1981) is as olivine tholeiite dragged from the Juan de Fuca ridge. It is composed of olivine phenocrysts in a groundmass of plagioclase, clinopyroxene and ilmenite. The experiments were performed in the range 500–900 °C and 1–5 kbar. The pseudosection was made to be comparable to the experiments with oxygen fugacity controlled by the quartz-fayalite-magnetite (QFM) buffer.

Nine runs overlap the conditions for which the pseudosection was calculated (Table S1). One characteristic of the pseudosection is that quartz and biotite are present in most fields (Fig. 2b), while neither biotite nor quartz were identified in the experimental runs. If these two phases are ignored, there is a good agreement between the experiments and the pseudosection, with only the lowest temperature run, at 498 °C, 5 kbar, presenting a mineral assemblage (hornblende + epidote + albite + sphene + quartz + biotite) different from the calculated one (hornblende + plagioclase + ilmenite + sphene).

4.3. Sample RM 29e

Sample RM 29e is an amphibolite from the Juscelândia Sequence, in the central part of the Brasilia Orogen (central Brazil). Works on the geology of this region and specifically on the Juscelêndia Sequence include Moraes and Fuck (1999), Dardenne (2000), Moraes et al. (2003), Valeriano et al. (2004) and Pimentel (2016). A thin section of this sample was described for this work, while the bulk composition was taken from Moraes et al. (2003). The reference conditions adopted are the pressure and temperature determined by Moraes and Fuck (1999). They used multi-equilibrium thermobarometry with THERMOCALC on a metapelite from the same unit as RM 29e, composed of garnet, staurolite, sillimanite, biotite, quartz, muscovite and plagioclase; and obtained 600 °C and 5.5 kbar.

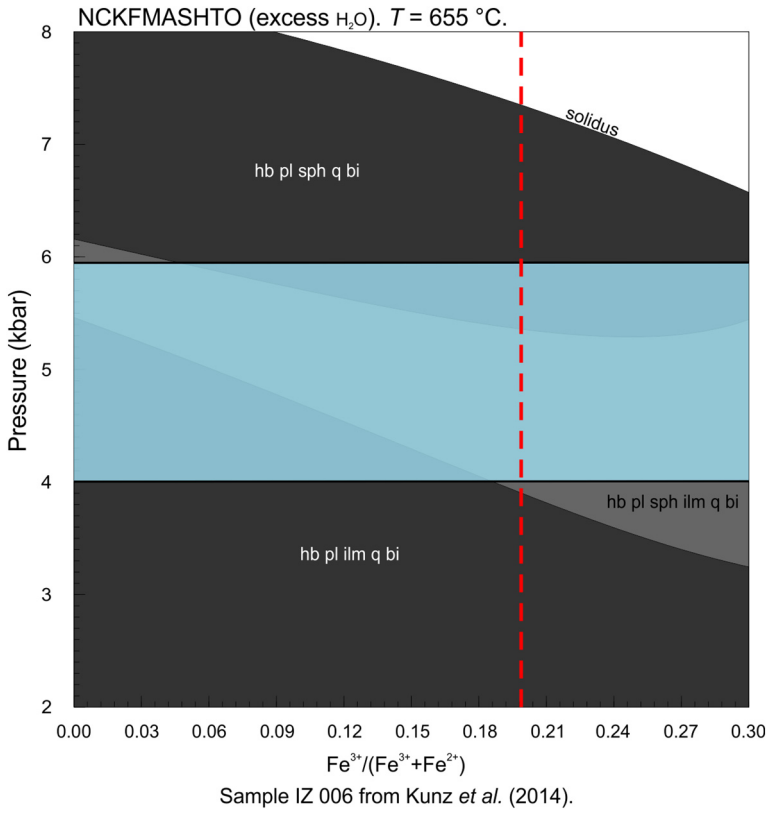

Fig. 6. P-X_{Fe3+} pseudosection calculated for the composition of sample IZ 006. The blue area represents the pressure at which the rock equilibrated, according to the calculations performed by Redler et al. (2012). The red dashed line represents the X_{Fe3+} value assumed in the P-T pseudosection for this sample (Fig. 2a). T = 655 °C. (For interpretation of the references to colour in this figure legend, the reader is referred to the web version of this article.)

Sample RM 29e is a fine-grained amphibolite with nematoblastic texture, which presents the assemblage hornblende + plagioclase + ilmenite + garnet + quartz ± carbonate. No carbonate-bearing equilibria was calculated, but carbonate is a minor phase (< 1%), and it was simply disregarded. At the reference conditions, the mineral assemblage, according to the pseudosection, would be hornblende + plagioclase + sphene + ilmenite + quartz + biotite (Fig. 3a). Even ignoring biotite, the observed mineral assemblage does not agree with what is calculated in the pseudosection. One of the mismatches is the absence of garnet in the calculated assemblage, so the pseudosection for this sample was calculated for a larger P range, up to 12 kbar. With this range, garnet does appear, but just at P > 11 kbar, associated with sphene and diopside. The other main difference is that, in the assumed conditions, sphene is calculated to be stable alongside ilmenite. Its stability field is calculated to extend up to 650 °C, in a way that it runs out only after diopside enters the assemblage. In short, the observed assemblage is not predicted to be stable anywhere in the covered P-T spectrum.

4.4. Sample SM 495

Sample SM 495 comes from the Votuverava Group, part of the southern Ribeira Fold Belt (southeastern Brazil). For information on regional geology, the reader is referred to Heilbron et al. (2004), Campanha et al. (2015), Faleiros et al. (2007, 2010, 2011) and references therein. A thin section of this sample was described for this work, while the composition was taken from Faleiros et al. (2011). The reference conditions adopted are the pressure and temperature determined by Yogi (2016) for a metapelite from the same unit as the mafic rock studied here. Yogi (2016) combined pseudosections calculated with Perple_X, multi-equilibrium calculations with THERMOCALC and the GASP barometer (Hodges & Crowley, 1985) to determine the conditions of formation of her sample as 620–650 °C and 6.0–7.0 kbar (see Fig. 7a). The bulk composition of the rock modelled by Yogi is given in table S2.

Sample SM 495 is medium-grained nematoblastic amphibolite composed mainly of prismatic to acicular hornblende and polygonal plagioclase, with sphene and epidote as accessories. At the reference conditions, the predicted mineral assemblage is hornblende + plagioclase + diopside + sphene + quartz (Figs. 3b, 7a). The observed mineral assemblage is different from the one predicted to be stable at the reference conditions, but, in this case, if quartz is ignored, the observed assemblage is predicted to be stable within the covered range, as a rather small field stretching from ≈ 490 to ≈ 515 °C and from ≈ 3 to ≈ 4.8 kbar. In Fig. 7a, the results of Yogi (2016) are superimposed on the pseudosection, and two stability fields are highlighted: the field of the assemblage described above and the field of the epidote-absent assemblage, hornblende + plagioclase + sphene + quartz (considered because of epidote low mode in the sample), which is larger, going from ≈500 to 675 °C, and from 2.2 to 4.0 kbar, at its largest P span, at ≈600 °C. In this latter, rather loose approximation, the temperature that would be inferred from the pseudosection agrees with the estimate made from the metapelite, while the pressure does not. The difference, in this case, would be that the modelling predicts the presence of diopside in the amphibolite. Diopside mode is predicted to increase with pressure increase, being over 6% at 7 kbar.

Since Fe^{3+} content is not constrained in this example, we calculated a P-X_{Fe3+} pseudosection (Fig. 7b) between X_{Fe3+} values of 0.0 and 0.3, at T = 640 °C, *i.e.* in the middle of the T interval defined by Yogi (2016). As in the previous examples in this work (Fig. 6) and in the literature (*e.g.* Diener and Powell, 2010), reducing X_{Fe3+} has the general effect of shifting phase boundaries up pressure. Although the observed assemblage is still not calculated to be stable at the same conditions estimated using the metapelites (6.1–7 kbar), at X_{Fe3+} = 0.09 the differences are

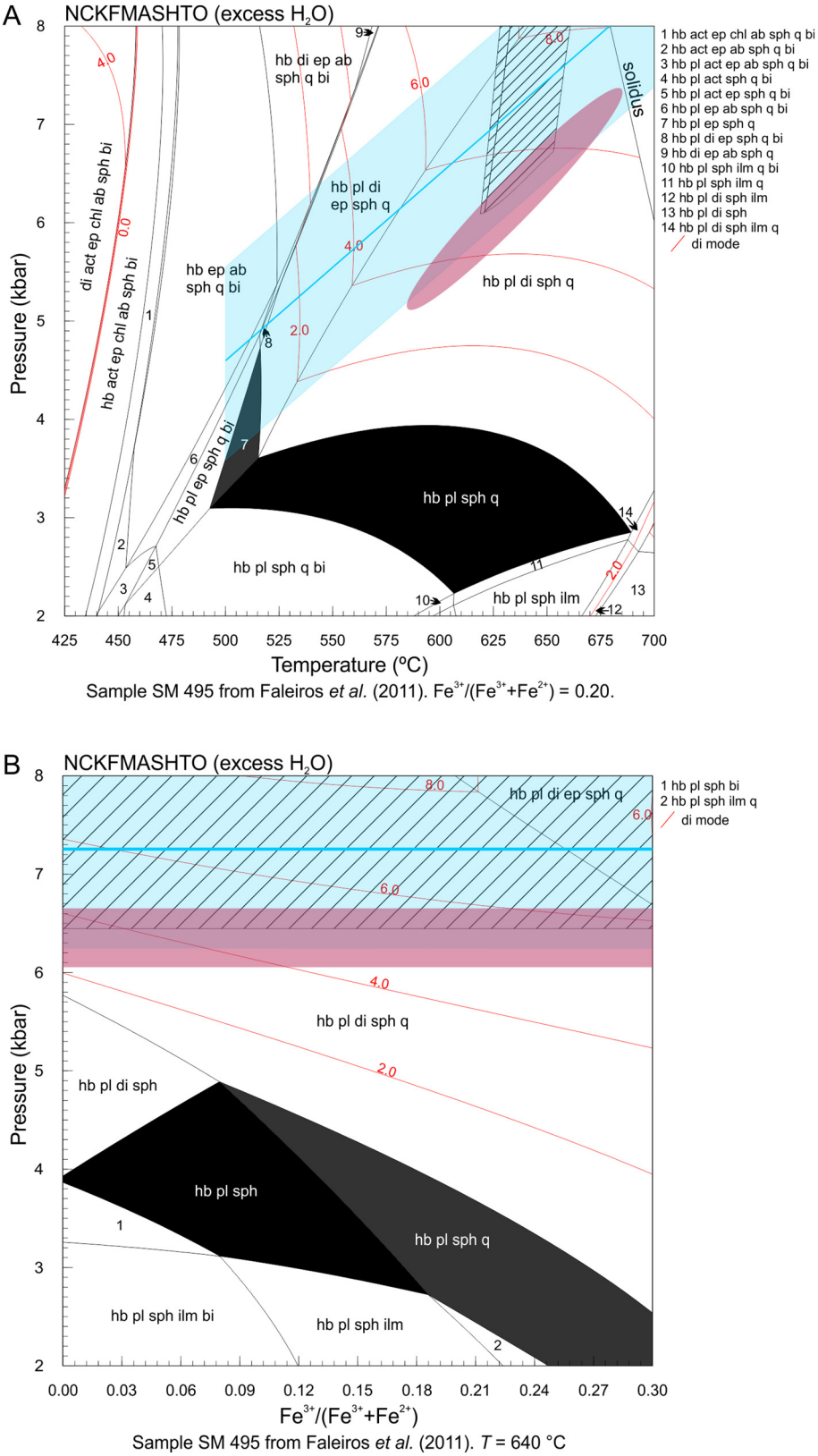

Fig. 7. (a). The *P-T* results obtained by Yogi (2016) superimposed on the pseudosection calculated for sample SM 495 (Fig. 3b). The hatched polygons represent the fields where the metapelite paragenesis is stable, the pink ellipse represents THERMOCALC averagePT result, and the blue line represents GASP barometer result, with the blue field representing its associated uncertainty. In the pseudosection, only the fields of the observed association are left colored. (b) A *P-*X_{Fe3+} pseudosection calculated for sample SM 495. The *P-T* results obtained by Yogi (2016) are superimposed, with the same symbology used in Fig. 7a. Again as in fig. 7a, only the fields of the observed association are left colored. (For interpretation of the references to colour in this figure legend, the reader is referred to the web version of this article.)

negligible, since quartz is absent and calculated diopside mode is about 2%.

4.5. Sample AL 83

The sample used in the experiments by Apted and Liou (1983) was a basaltic glass from the Juan de Fuca Ridge. The experiments were carried out in the range 400–700 °C, 5–7 kbar, thus mostly overlapping the *P-T* range considered in this work (table S3). Two pseudosections were calculated, one whose X_{Fe3+} makes it comparable to the experiments with oxygen fugacity controlled by the quartz-fayalite-magnetite (QFM) buffer (Fig. 4a) and a second one, comparable to the experiments with oxygen fugacity controlled by the nickel-nickel oxide (NNO) buffer (Fig. 8). Despite the fact that Apted and Liou (1983) briefly discuss the phase relations between the Ti-bearing phases, sphene and ilmenite, they are not explicitly accounted for as run products in their run table (their table 7, page 336), so the presence or absence of ilmenite and sphene will not be discussed here.

In general terms, the pseudosections for AL 83 predict typical amphibolite facies minerals, such as hornblende, plagioclase and diopside, to be stable at lower temperatures than those indicated by the experimental data (Figs. 4a, 8), while experimental data indicate typical greenschist facies minerals, specially epidote and albite, to be stable at higher temperatures than those predicted in the pseudosections. Both pseudosections show diopside to be stable throughout the covered *P-T* range (Figs. 4a, 8), while none of the runs produced it, regardless of the f_{O2} buffer utilized. For the pressures at which the experiments were carried out both pseudosections predict hornblende to be stable at temperatures as low as 460 °C, while in the experiments the lowest temperatures at which hornblende was produced were 600 °C (7 kbar/QFM), 575 °C (7 kbar/NNO) and 525 °C (5 kbar/NNO); plagioclase is predicted in the pseudosections to be stable at temperatures higher than 530–560 °C, while in the experiments it was produced only in the highest temperature runs, at 7 kbar/700 °C (QFM) and 7 kbar/700 °C and 5 kbar/650 °C (NNO). The runs at 675 °C (7 kbar/QFM), 700 °C (7 kbar/QFM) and 700 °C (5 kbar/NNO) fall in the suprasolidus field of the corresponding pseudosections, but no melt was detected in the experiments.

Epidote was produced in all but one of the considered runs, at 650 °C (5 kbar/NNO), while the pseudosections predict it to be stable up to 525 °C (7 kbar/ "QFM" pseudosection), 560 °C (7 kbar/ "NNO" pseudosection) and 530 °C (5 kbar/ "NNO" pseudosection). Albite, in turn, was obtained in the experiments at temperatures 70–100 °C higher than the stability fields predicted in the pseudosections.

4.6. Sample RM 201

Like sample RM 29e, sample RM 201 comes from the Juscelândia Sequence (see above for more information) and the reference conditions are the same as the ones adopted for RM 29e (600 °C; 5.5 kbar). Sample RM 201 is a medium-grained amphibolite that presents the mineral assemblage hornblende + plagioclase + sphene + ilmenite. At the reference conditions, the stable mineral assemblage according to the pseudosection would be hornblende + plagioclase + diopside + albite + sphene + biotite (Fig. 4b). Ignoring, quartz and biotite, the main mismatch between the observed mineral assemblage and the calculated pseudosection is the presence of diopside. In fact, as stressed before, diopside is calculated to be stable along all the covered *P-T* range, so that the observed mineral assemblage is not calculated to be stable anywhere in the pseudosection. Other discrepancies include the absence of ilmenite and presence of sphene in the calculated assemblage at the *P-T* conditions calculated by Moraes and Fuck (1999).

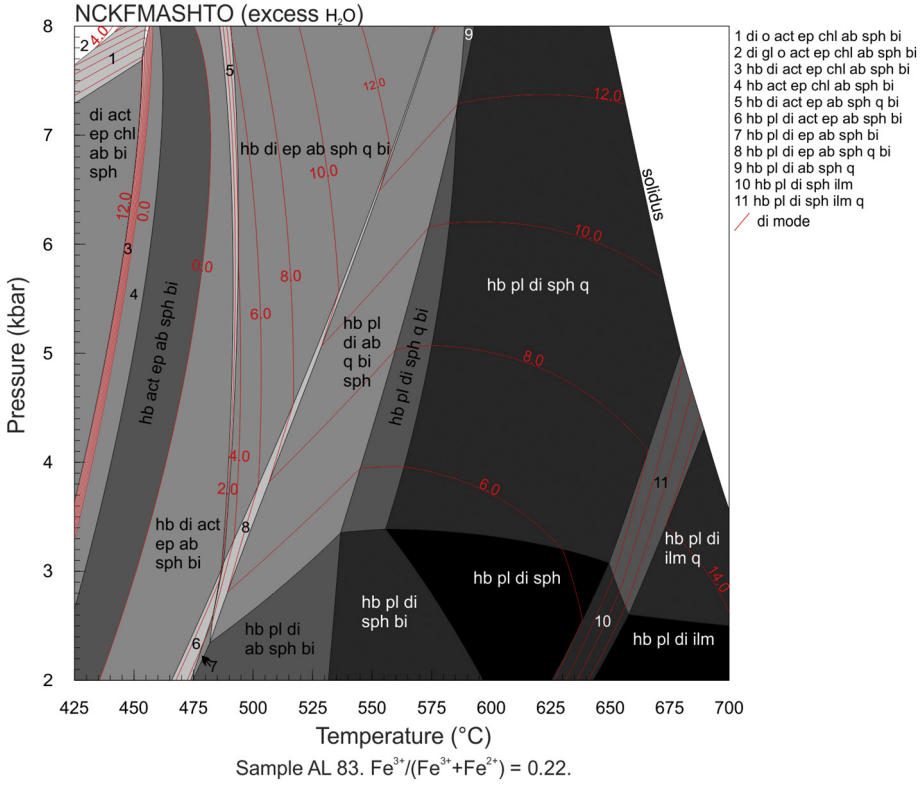

Fig. 8. *P-T* pseudosections calculated for sample AL 83, with $X_{Fe3+} = 0.22$, value chosen to make the pseudosection comparable to the experiments whose oxygen fugacity was controlled by the NNO buffer.

5. Discussion

5.1. Garnet stability

In the discussion of the results for sample RM 29e, it was shown that there is a difference of 5.5 kbar between the reference pressure and the lowest pressure at which garnet is predicted to be formed at the pseudosection. Of course, there are uncertainties in the data we used for comparison (see below, also *Introduction*), but this is a large difference, and, in calculations using this set of activity composition models it is common for garnet to be predicted in this range of pressures, as exemplified by the absence of garnet in all the other pseudosections calculated in this work (see also Green et al., 2016). This is in contradiction not only with the data presented here, but also with other occurrences (*e.g.* Laird, 1980). The most likely cause to this difference is the absence of Mn in the activity-composition models, since Mn is usually strongly partitioned into garnet (Deer et al., 1982). Several studies show, for metapelitic systems, that the inclusion of Mn expands the predicted stability field of garnet to lower temperature and pressure (Droop and Harte, 1995; Mahar et al., 1997; Spear and Cheney, 1989; Symmes & Ferry, 1992). It is noteworthy, however, that there are no studies that evaluate this effect in mafic compositions.

In an attempt to evaluate the influence of other compositional factors, we calculated a pseudosection where the composition of RM 29e (the one garnet-bearing sample) is enriched in Al_2O_3 and total iron. The reasoning was to push Al_2O_3 to the values observed in high-alumina basalts (*e.g.* Crawford et al., 1987) and total iron to values observed in tholeiitic ferro-basalts (*e.g.* Brooks et al., 1991; Toplis and Carrol, 1996) with the constraint of silica not being lowered below 45% (the lower limit of basic rocks in the diagram of Le Maitre et al., 1989). The final composition used is given in table S4. This diagram (Fig. 9) shows that, although predicted garnet stability is expanded down pressure along such a compositional vector, garnet is still not calculated to be stable at the reference pressure for this sample and, with effect, it is predicted to be stable alongside plagioclase (thus forming a garnet amphibolite) only in the extreme of the diagram, with both Al_2O_3 and FeO (total) above 18 wt%. Thus, this diagram support our point on the influence of MnO.

Though almandine is usually the dominant end-member in garnet from metamafic rocks, grossular and pyrope are important as well (Deer et al., 1982). It means that the presence or absence of garnet affects the stability and mode of all main constituents of metamafic rocks in these pseudosections, because if its components are not being "used" to form garnet, they will be available to stabilize other phases, like diopside and epidote (*e.g.* Forshaw et al., 2019). White et al. (2014b), working with thermodynamic modelling of metapelitic systems, pointed out that, with exception for the addition of garnet, there is little difference between the mineral assemblages calculated to be stable in Mn-bearing and Mn-free systems. An equivalent study about the influence of Mn on mafic systems is still to be undertaken, though.

5.2. Clinopyroxene and hornblende stability

In four of the pseudosections calculated here diopside is stable at greenschist facies conditions, and, in fact, in two of them it is stable all along the covered *P-T* range. These features occur along with overestimation stability field of hornblende and with predicted omphacite stability at pressures as low as ≈ 6 kbar, at $T = 425–450$ °C. Diopside mode contours show that calculated diopside amounts are significant (up to 20%) and the highest modes occur at the lowest temperatures considered. Diopside and hornblende stability under such low temperatures is in disagreement not only with experimental and thermobarometric calculations specific to the studied samples, but also with mineral assemblages observed in mafic rocks in general (*e.g.* Apted and Liou, 1983; Bevins and Robinson, 1993; Cooper and Lovering, 1970; Laird, 1980; Spear, 1981, 1982; Wiseman, 1934) and, although not investigated in detail here, omphacite predicted stability in this rocks seems to be overestimated as well (Ernst, 1973, Brothers and

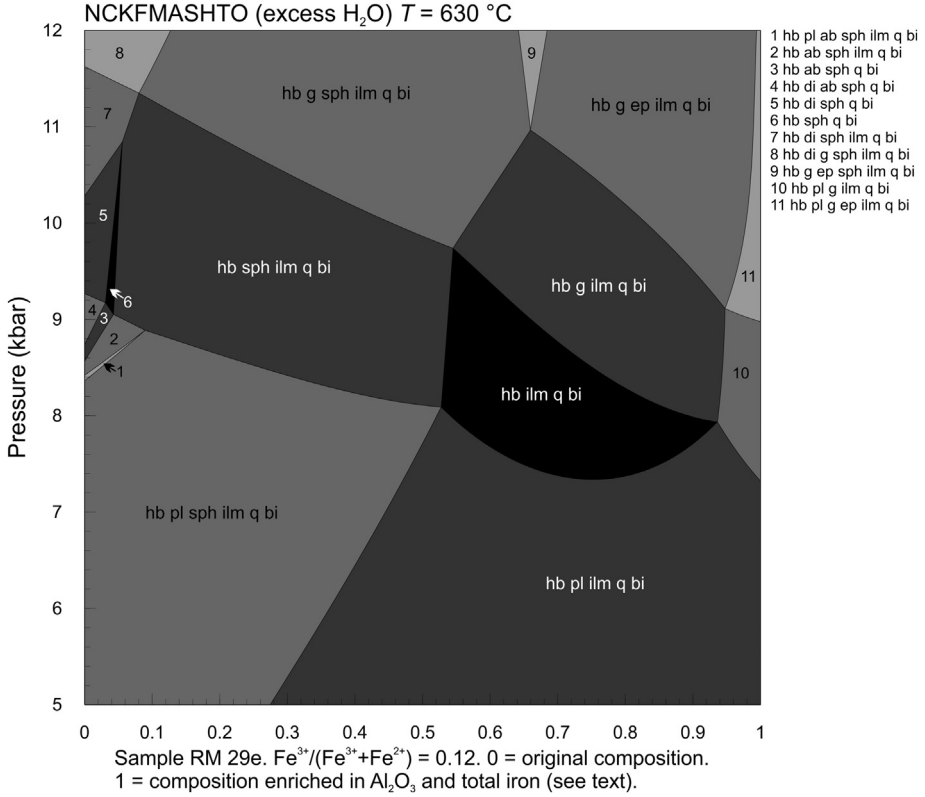

Fig. 9. A *P*-x pseudosection where 0 correspond to the composition of sample RM 29e and 1 correspond to the same composition enriched in Al_2O_3 and total iron.

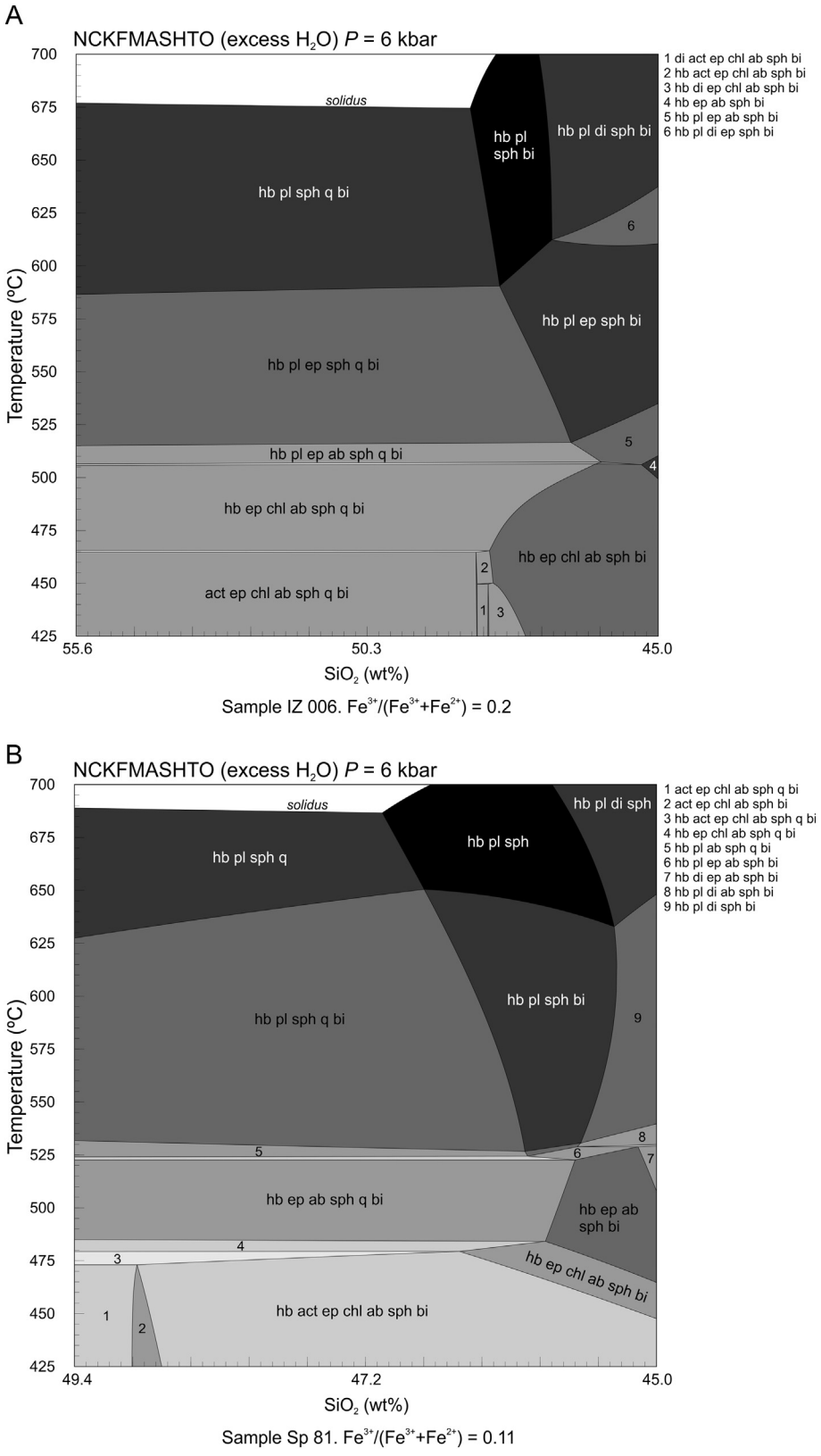

Fig. 10. (a) A *T*-x pseudosection calculated for sample IZ 006, with SiO_2 quantity decreasing from left to right. (b) A *T*-x pseudosection calculated for sample Sp 81, with SiO_2 quantity decreasing from left to right.

Yokoyama, 1982; Evans, 1990<!——>; Bucher and Grapes, 2011. The comparison with the other investigated). Bulk-rock compositions (Fig. 1) indicate that these features are mainly related to SiO_2 content: Figs. 10 and 11 show *T*-SiO_2 content pseudosections calculated for the compositions of samples IZ 006, Sp 81, RM 29e and RM 201. In the first three cases SiO_2 content was decreased to 45% (the limit between basic and ultrabasic rocks in the diagram of Le Maitre et al., 1989) while in the last one (in which greenschist facies diopside was originally

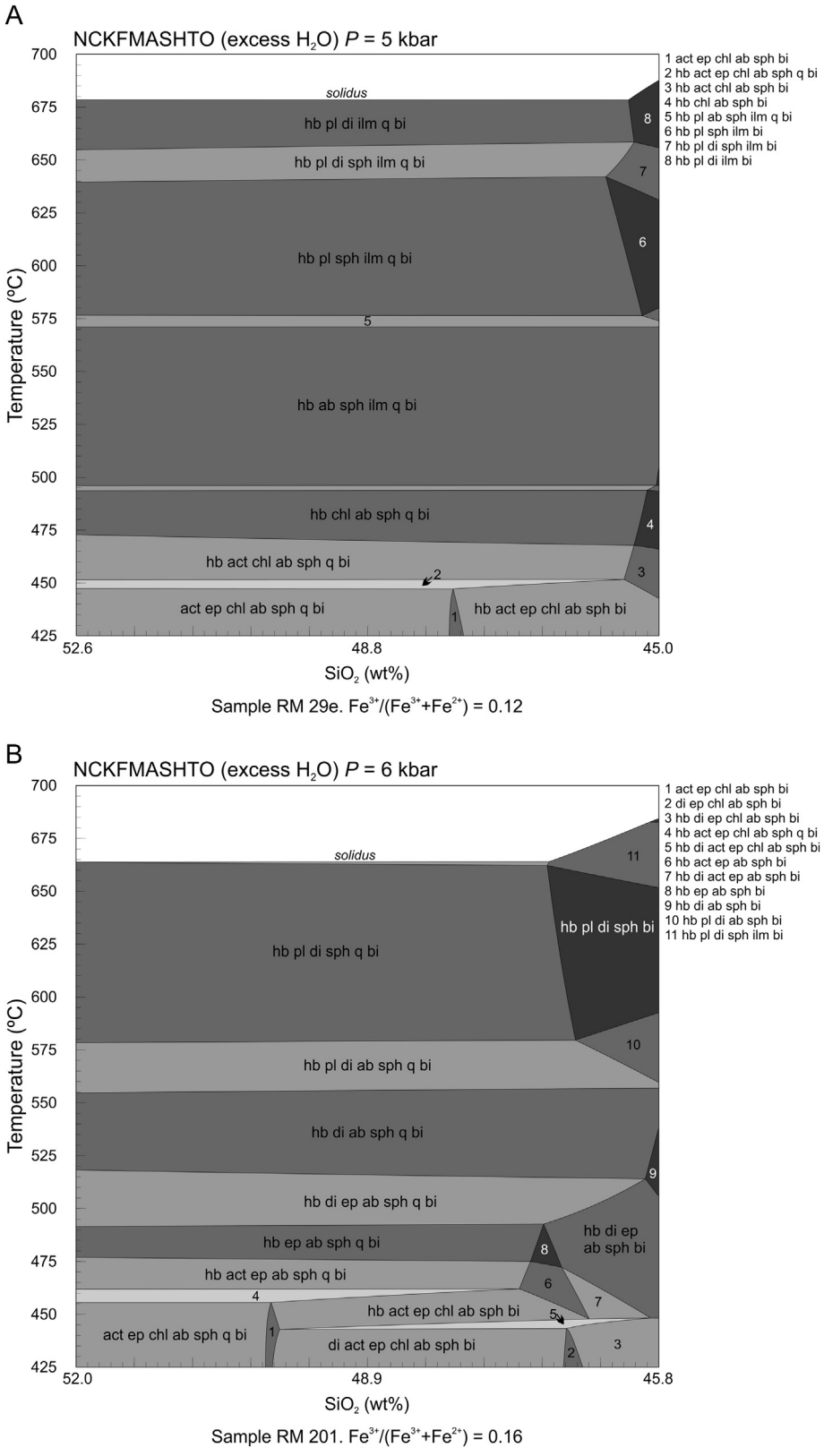

Fig. 11. (a) A *T*-x pseudosection calculated for sample RM 29e, with SiO_2 quantity decreasing from left to right. (b) A *T*-x pseudosection calculated for sample RM 201, with SiO_2 quantity increasing from left to right.

predicted) SiO_2 content was raised to the arbitrary value of 52%. In the case of RM 201 (Fig. 11b), at SiO_2 contents above ≈ 50% quartz is predicted to be stable, and low-grade diopside- and hornblende-bearing assemblages are not, as the full predicted assemblage becomes actinolite + epidote + chlorite + albite + sphene + quartz, just as is the case for samples IZ 006, Sp 01 and RM 29e.

The other three pseudosections show somewhat different stories: in all three, the predicted stability field of hornblende is enlarged after

quartz becomes unstable, but only in the case of IZ 006 low temperature diopside is also predicted to be stable, and even so, only at a limited SiO_2 range (≈47–48 wt%). So, although these issues are certainly related to SiO_2 content, there are other factors at play. In fact, in the case of RM 201, despite the fact that raising SiO_2 raises the temperature at which diopside is predicted to be stable, this rise (to 492 °C, at 6 kbar) is too small.

Diopside stability at low temperatures is not a problem *per se*, as it is recorded, for example, in metaultramafic rocks (Evans, 1977; Trommsdorff and Evans, 1972) which are poorer in SiO_2 than metamafic rocks. However, in the case of mafic rocks, diopside stability in such low temperatures is clearly wrong. The cause of this behavior in the activity-composition models is hard to unravel. The activity-composition models used here (Green et al., 2016; White et al., 2014a; see also Powell et al., 2014) were designed to work as set, meaning that a discrepancy in some calculation can be related to any of the models, or to the relationships between two or more of them. Forshaw et al. (2019), working with upper amphibolite- and granulite-facies mafic rocks, found discrepancies between observed clinopyroxene and hornblende compositions and compositions calculated using THERMOCALC and the same activity-composition models used here. They point out several causes for these mismatches, including incorrect partitioning of Fe^{2+} and Mg between clinopyroxene and amphibole and a "direct" overstabilization of Al-rich hornblende (*i.e.* a problem in the amphibole activity-composition model). It is possible that the issues pointed out by Forshaw et al. (2019) and the ones pointed out here are related, but our data do not allow this possibility to be evaluated.

5.3. Other discrepancies

Besides the problems discussed above, there are other, minor discrepancies that have been found. One such discrepancy is the presence of biotite: it was detected only in IZ 006, but is predicted to be stable at the reference conditions in all but one natural sample (SM 495) and in most relevant experimental conditions. In the case of the experiments, it may have been overlooked, or may not have nucleated, as predicted modes are always very low, below 1%. In the case of natural samples RM 201 and RM 29e the situation is different, as predicted biotite modes, at the reference conditions, are between 3 and 5%. The compositions studied here are K_2O-poor (as are mafic rocks in general) and, at greenschist and amphibolite conditions biotite is typically the one phase that has K_2O as an essential component. So, biotite stability will depend on the relationship between bulk K_2O content and how much K_2O is taken by other phases, what, in this case, means mainly hornblende and plagioclase. As both examples have issues related to major phases (diopside in the case of RM 201, garnet in the case of RM 29e) that certainly have an effect, at the very least, on predicted modes of plagioclase and hornblende, it is likely that predicted biotite stability is linked to the same issues pointed before. This cannot be affirmed with certainty, though.

Another discrepancy refers to predicted quartz stability in samples SM 495, AL 83 and Sp 81, where it was not observed. In the case of SM 495, its mode is low, and, as discussed above, with slightly lower X_{Fe3+} it is not predicted to be stable, while, in the case of AL 83 quartz predicted stability is linked to other issues discussed previously. As for Sp 81, predicted quartz mode is below 1% in the 3 kbar experiments, but may be as high as 5% in the conditions of the 5 kbar experiments. Given the simple nature of the predicted and observed assemblages (see table S3), the predicted stability of quartz have to be linked to predicted compositions of either plagioclase or hornblende or both being too SiO_2-poor. This cannot be verified, though, as the compositions of the products of these runs are not explicitly accounted in Spear (1981) (see their table 3, page 702).

Finally, three experimental runs from Apted and Liou (1983) fall in the suprasolidus field of the corresponding pseudosections. The position of the solidus curve was one of the main points of the study by Green et al. (2016), so it seems likely that the models are correct in this regard.

6. Conclusions

The activity-composition models developed by Green et al. (2016), based on previous work by Diener et al. (2007) and Green et al. (2007), have been successful in describing the metamorphism of rocks of broad mafic composition, as can be seen in several works (Palin and White, 2016; Schorn, 2018; Tang et al., 2017; White et al., 2017). Specifically in this work, predictions based on pseudosections for mafic rocks agree (mostly) with the data used for comparison in three out of the six studied examples. In the cases where there are mismatches, part of them are minor, sample-specific differences, that can, actually, be indicative of problems in the data used for comparison as much as problems in the activity-composition models used for construction of the pseudosections. However, most of the mismatches verified here are related to issues where the activity-composition models are clearly at fault, namely the stability fields of garnet and diopside and hornblende. While the absence of manganese in the activity-composition models is easily identified as a very likely cause of the problem of the garnet stability field, the overestimation of the stability fields of diopside and hornblende is a quite different and more complex problem, for which we do not have an answer. Nonetheless, the data shows that this behavior is linked to SiO_2 content, and also that there *are* other factors at play. It should be stressed that this kind of problem cannot, in principle, be worked around simply by ignoring the phases at issue, because components either being (or not being) "used" in these phases will either be unavailable or be available "in excess" to other phases, thus affecting their mode, composition and stability fields. Researchers should be aware of these issues when modelling SiO_2-poor and garnet-bearing low- to medium-grade metamafic rocks.

Despite, the enormous advances made in metamorphic petrology in the recent years, *P-T* estimates must always be seen critically, and the methods used for thermobarometric estimates should be thoroughly tested.

Acknowledgements

The authors thank F. Faleiros and T. Yogi for the access to their material and data, M. Hueck for his help with sample selection and C. Yakymchuk and P. Lanari for their extensive and helpful revisions. R. White and J. Diener are thanked for revision of an earlier version of the manuscript, and for various helpful comments. We also thank D. Pattison and J. Forshaw for some fruitful discussions. The study was supported by FAPESP (processes n° 13/04007-0 and 16/22627-3). C. A. Santos received a PhD scholarship from CNPq.

Appendix A. Supplementary data

Supplementary data to this article can be found online at https://doi.org/10.1016/j.lithos.2019.04.024.

References

Apted, M.J., Liou, J.G., 1983. Phase relations amongst greenschist, epidote-amphibolite, and amphibolite in a basaltic system. Am. J. Sci. 283A, 328–354.
Bevins, R.E., Robinson, D., 1993. Parageneses of Ordovician sub-greenschist to greenschist facies metabasites from Wales, U.K. Eur. J. Mineral. 5, 925–935.
Brooks, C.K., Larsen, L.M., Nielsen, T.F.D., 1991. Importance of iron-rich tholeiitic magmas at divergent plate margins: a reappraisal. Geology. 19, 269–272.
Brothers, R.N., Yokoyama, K., 1982. Comparison of the high-pressure schist belts of New Caledonia and Sanbagawa, Japan. Contrib. Mineral. Petrol. 79, 219–229.
Bucher, K., Grapes, R., 2011. Petrogenesis of Metamorphic Rocks. Springer-Verlag. 428p, Heidelberg.
Campanha, G.A.C., Faleiros, F.M., Basei, M.A.S., Tassinari, C.C.G., Nutman, A.P., Vasconcelos, P.M., 2015. Geochemistry and age of mafic rocks from Votuverava Group, Southern Ribeira Belt, Brazil: evidence for 1490 Ma oceanic back-arc magmatism. Precambrian Res. 266, 530–550.

Connolly, J.A.D., Petrini, K., 2002. An automated strategy for calculation of phase diagram sections and retrieval of rock properties as a function of physical conditions. J. Metamorph. Geol. 20, 697–708.

Cooper, A.F., Lovering, J.F., 1970. Greenschist amphiboles from Haast River, New Zealand. Contrib. Mineral. Petrol. 27, 11–24.

Crawford, A.J., Falloon, T.J., Eggins, S., 1987. The origin of island arc high-alumina basalts. Contrib. Mineral. Petrol. 97, 417–430.

Dardenne, M.A., Cordani, U.G., Milani, E.J., Thomaz Filho, A., Campos, D.A., 2000. The Brasília Fold Belt. Tectonic evolution of South America. Rio de Janeiro, pp. 231–263.

de Capitani, C., Brown, T.H., 1987. The computation of chemical equilibrium in complex systems containing non-ideal solutions. Geochim. Cosmochim. Acta 51, 2639–2652.

Deer, W.A., Howie, R.A., Zussman, J., 1982. Rock forming Minerals v.1A. Geological Society, London 917p.

Diener, J.F.A., Powell, R., 2010. Influence of ferric iron on the stability of mineral assemblages. J. Metamorph. Geol. 28, 599–613.

Diener, J.F.A., Powell, R., 2012. Revised activity-composition models for clinopyroxene and amphibole. J. Metamorph. Geol. 30, 131–142.

Diener, J.F.A., Powell, R., White, R.W., Holland, T.J.B., 2007. A new thermodynamic model for clino- and orthoamphiboles in the system Na_2O-CaO-FeO-MgO-SiO_2-H_2O-O. J. Metamorph. Geol. 25, 631–656.

Droop, G.T.R., Brodie, K.H., 2012. Anatectic melt volumes in the thermal aureole of the Etive complex, Scotland: the roles of fluid-present and fluid-absent melting. J. Metamorph. Geol. 30, 843–864.

Droop, G.T.R., Harte, B., 1995. The effect of Mn on the phase relations of medium-grade pelites: constraints from natural assemblages on petrogenetic grid topology. J. Petrol. 36, 1549–1578.

Ernst, W.G., 1973. Blueschist metamorphism and P-T regimes in active subduction zones. Tectonophysics. 17, 255–272.

Evans, B.W., 1977. Metamorphism of alpine peridotite and serpentine. Annu. Rev. Earth Planet. Sci. 5, 397–447.

Evans, B.W., 1990. Phase relations of epidote-blueschists. Lithos. 25, 3–23.

Faleiros, F.M., Campanha, G.A.C., Bello, R.M.S., Fuzikawa, K., 2007. Fault-valve actionand vein development during strike-slip faulting: an example from the Ribeira Shear Zone, Southeastern Brazil. Tectonophysics. 438, 1–32.

Faleiros, F.M., Campanha, G.A.C., Bello, R.M.S., Fuzikawa, K., 2010. Quartz recrystallization regimes, c-axis texture transitions and fluid inclusion reequilibration in a prograde greenschist to amphibolite facies mylonite zone (Ribeira Shear Zone, SE Brazil). Tectonophysics. 485, 193–214.

Faleiros, F.M., Ferrari, V.C., Costa, V.S., Campanha, G.A.C., 2011. Geoquímica e petrogênese de metabasitos do Grupo Votuverava (Terreno Apiaí, Cinturão Ribeira Meridional): Evidências de uma bacia retroarco calimiana. Geol. USP-Sér. Cient. 11, 135–155.

Forshaw, J.B., Waters, D.J., Pattison, D.R.M., Palin, R.M., Gopon, P., 2019. A comparison of observed and thermodynamically predicted phase equilibria and mineral compositions in mafic granulites. J. Metamorph. Geol. 37, 153–179.

Grant, J.A., 2009. Thermocalc and experimental modelling of melting of pelite, Morton Pass, Wyoming. J. Metamorph. Geol. 27, 571–578.

Green, E.C.R., Holland, T.J.B., Powell, R., 2007. An order-disorder model for omphacitic pyroxenes in the system jadeite–diopside–hedenbergite–acmite, with applications to eclogitic rocks. Am. Mineral. 92, 1181–1189.

Green, E.C.R., White, R.W., Diener, J.F.A., Powell, R., Holland, T.J.B., Palin, R.M., 2016. Activity-composition relations for the calculation of partial melting equilibria in metabasic rocks. J. Metamorph. Geol. 34, 845–869.

Handy, M.R., Franz, L., Heller, F., Janott, B., Zurbriggen, R., 1999. Multistage accretion and exhumation of the continental crust (Ivrea crustal section, Italy and Switzerland). Tectonics. 18, 1154–1177.

Heilbron, M., Pedrosa-Soares, A.C., Campos Neto, M.C., Silva, L.C., Trouw, R.A.J., Janasi, V.A., 2004. Província Mantiqueira. In: Mantesso-Neto, V., Bartoreli, A., Carneiro, C.D.R., Brito-Neves, B.B. (Eds.), Geologia do continente sul-americano: evolução da obra de Fernando Flávio Marques de Almeida. São Paulo. Beca, pp. 231–235.

Henk, A., Franz, L., Teufel, S., Oncken, O., 1997. Magmatic underplating, extension, and crustal reequilibration: insights from a cross-section through the Ivrea Zone and Strona-Ceneri Zone, Northern Italy. J. Geol. 105, 367–377.

Hodges, K.V., Crowley, P.D., 1985. Error estimation and empirical geothermobarometry for pelitic systems. American Mineralogist. 70, 702–709.

Holland, T.J.B., Powell, R., 2003. Activity-composition relations for phases in petrological calculations: an asymmetric multicomponent formulation. Contrib. Mineral. Petrol. 145, 492–501.

Holland, T.J.B., Powell, R., 2011. An improved and extended internally consistent thermodynamic dataset for phases of petrological interest, involving a new equation of state for solids. J. Metamorph. Geol. 29, 333–383.

Korhonen, F.J., Clark, C., Brown, M., Taylor, R.J.M., 2014. Taking the temperature of the hottest crust. Earth Planet. Sci. Lett. 408, 341–354.

Kunz, B.E., Johnson, T.E., White, R.W., Redler, C., 2014. Partial melting of metabasic rocks in Val Strona di Omegna, Ivrea Zone, northern Italy. Lithos. 190 (191), 1–12.

Laird, J., 1980. Phase equilibria in mafic schist from Vermont. J. Petrol. 21, 1–37.

Lanari, P., Duesterhoeft, E., 2019. Modeling metamorphic rocks using equilibrium thermodynamics and internally consistent databases: past achievements, problems and perspectives. J. Petrol. 60, 19–56.

Lanari, P., Riel, N., Guillot, S., Vidal, O., Schwartz, S., Pêcher, A., Hattori, K.A., 2013. Deciphering high-pressure metamorphism in collisional context using microprobe mapping methods: application to the Stak eclogitic massif (northwest Himalaya). Geology. 41, 111–114.

Le Maitre, R.W., 1976. The chemical variability of some common igneous rocks. J. Petrol. 17, 589–598.

Le Maitre, R.W., Bateman, P., Dudek, A., Keller, J., Le Bas, M.J.L., Sabine, P.A., Zannetin, B., 1989. A classification of igneous rocks and glossary of terms. Blackwell, Oxford, p. 236p.

Lecuyer, C., Ricard, Y., 1999. Long-term fluxes and budget of ferric iron: implication for the redox states of the Earth's mantle and atmosphere. Earth Planet. Sci. Lett. 165, 197–211.

Luvizotto, G.L., Zack, T., 2009. Nb and Zr behavior in rutile during high-grade metamorphism and retrogression: an example from the Ivrea-Verbano Zone. Chem. Geol. 261, 303–317.

Mahar, E.M., Baker, J.M., Powell, R., Holland, T.J.B., Howell, N., 1997. The effect of Mn on mineral stability in metapelites. J. Metamorph. Geol. 15, 223–238.

Moraes, R., Fuck, R.A., 1999. Trajetória PT horária para o metamorfismo da Sequência Juscelândia, Goiás: condições do metamorfismo e implicações tectônicas. Rev. Bras. Geo. 29, 603–612.

Moraes, R., Fuck, R.A., Pimentel, M.M., Gioia, S.M.C.L., Figueiredo, A.M.G., 2003. Geochemistry and Sm-Nd isotopic characteristics of bimodal volcanic rocks of Jescelândia Sequence, Goiás, Brazil: Mesoproterozoic transition from continental rift to ocean basin. Precambrian Res. 125, 317–336.

Palin, R.P., White, R.W., 2016. Emergence of blueschists on Earth linked to secular changes in oceanic crust composition. Nat. Geosci. 9, 60–65.

Pimentel, M.M., 2016. The tectonic evolution of the Neoproterozoic Brasília Belt, central Brazil: a geochronological and isotopic approach. Brazilian Journal of Geology 46, 67–82.

Powell, R., Holland, T.J.B., 1988. An internally consistent dataset with uncertainties and correlations: 3. Applications to geobarometry, worked examples and a computer program. J. Metamorph. Geol. 6, 173–204.

Powell, R., Holland, T.J.B., 2008. On thermobarometry. J. Metamorph. Geol. 26, 155–179.

Powell, R., Holland, T.J.B., Worley, B., 1998. Calculating phase diagrams involving solid solutions via non-linear equations, with examples using THERMOCALC. J. Metamorph. Geol. 16, 577–588.

Powell, R., Guiraud, M., White, R.W., 2005. Truth and beauty in metamorphic phase equilibria: conjugate variables and phase diagrams. Can. Mineral. 43, 21–33.

Powell, R., White, R.W., Green, E.C.R., Holland, T.J.B., Diener, J.F.A., 2014. On parameterizing thermodynamic descriptions of minerals for petrological calculations. J. Metamorph. Geol. 32, 245–260.

Redler, C., Johnson, T.E., White, R.W., Kunz, B.E., 2012. Phase equilibrium constraints on a deep crustal metamorphic field gradient: metapelitic rocks from the Ivrea Zone (NW Italy). J. Metamorph. Geol. 30, 235–254.

Schmid, S.M., Zingg, A., Handy, M., 1987. The kinematics of movements along the Insubric Line and the emplacement of the Ivrea Zone. Tectonophysics. 135, 47–66.

Schorn, S., 2018. Dehydration of metapelites during high-P metamorphism: the coupling between fluid sources and fluid sinks. J. Metamorph. Geol. 36, 369–391.

Sinigoi, S., Quick, J.E., Demarchi, G., Kloetzli, U., 2011. The role of crustal fertility in the generation of large silicic magmatic systems triggered by intrusion of mantle magma in the deep crust. Contrib. Mineral. Petrol. 162, 691–707.

Spear, F.S., 1981. An experimental study of hornblende stability and compositional variability in amphibolite. Am. J. Sci. 281, 697–934.

Spear, F.S., 1982. Phase equilibria of amphibolites from the Post Pond Volcanics, Mt. Cube Quadrangle, Vermont. J. Petrol. 23, 383–427.

Spear, F.S., Cheney, J.T., 1989. A petrogenetic grid for pelitic schists in the system SiO_2-Al_2O_3-FeO-MgO-K_2O-H_2O. Contrib. Mineral. Petrol. 101, 149–164.

Symmes, G.H., Ferry, J.M., 1992. The effect of whole-rock MnO content on the stability of garnet in pelitic schists during metamorphism. Journal of Metamorphic Geology 10, 221–237.

Tang, L., Santosh, M., Tsunogae, T., Koizumi, T., Hu, X., Teng, X.M., 2017. Petrology, phase equilibria modelling and zircon U–Pb geochronology of Paleoproterozoic mafic granulites from the Fuping Complex, North China Craton. J. Metamorph. Geol. 35, 517–540.

Tibaldi, A.M., Álvarez-Valero, A.M., Otamendi, J.E., Cristofollini, E.A., 2011. Formation of paired pelitic and gabbroic migmatites: Na empirical investigation of the consistency of geothermometers, geobarometers and pseudosections. Lithos. 122, 57–75.

Toplis, M.J., Carrol, M.R., 1996. Differentiation of ferro-basaltic magmas under conditions open and closed to oxygen. Implications for the Skaergard Intrusion and other natural systems. J. Petrol. 37, 837–858.

Trommsdorff, V., Evans, B.W., 1972. Progressive metamorphism of antigorite schist in the Bergell tonalite aureole (Italy). Am. J. Sci. 272, 487–509.

Tual, L., Möller, C., Whitehouse, M.J., 2018. Tracking the prograde *P–T* path of Precambrian eclogite using Ti-in-quartz and Zr-in-rutile geothermobarometry. Contrib. Mineral. Petrol. 173, 56.

Valeriano, C.M., Dardenne, M.A., Fonseca, M.A., Simões, L.S.A., Seer, H.J., 2004. A Evolução tectônica da Faixa Brasília. In: Mantesso-Neto, V., Bartoreli, A., Carneiro, C.D.R., Brito-Neves, B.B. (Eds.), Geologia do continente sul-americano: evolução da obra de Fernando Flávio Marques de Almeida. São Paulo. Beca, pp. 575–592.

Weinberg, R.F., Hasalová, P., 2015. Water-fluxed melting of the continental crust: a review. Lithos. 212-215, 158–188.

White, R.W., Powell, R., Holland, T.J.B., Worley, B.A., 2000. The effect of TiO_2 and Fe_2O_3 on metapelitic assemblages at greenschist and amphibolite facies conditions: mineral equilibria calculations in the system K_2O–FeO–MgO–Al_2O_3–SiO_2–H_2O–TiO_2–Fe_2O_3. J. Metamorph. Geol. 18, 497–511.

White, R.W., Powell, R., Clarke, G.L., 2002. The interpretation of reaction textures in Fe-rich metapelitic granulites of the Musgrave Block, central Australia: constraints from mineral equilibria calculations in the system K_2O-FeO-MgO-Al_2O_3-SiO_2-H_2O-TiO_2-Fe_2O_3. J. Metamorph. Geol. 20, 41–55.

White, R.W., Stevens, G., Johnson, T.E., 2011. Is the crucible reproducible? Reconciling melting experiments with thermodynamic calculations. Elements. 7, 241–246.

White, R.W., Powell, R., Johnson, T.E., 2014a. The effect of Mn in mineral stability in metapelites revisited: new *a-x* relations for manganese-bearing minerals. J. Metamorph. Geol. 32, 809–828.
White, R.W., Powell, R., Holland, T.J.B., Johnson, T.E., Green, E.C.R., 2014b. New mineral activity-composition relations for thermodynamic calculations in metapelitic systems. J. Metamorph. Geol. 32, 261–286.
White, R.W., Palin, R.M., Green, E.C.R., 2017. High-grade metamorphism and partial melting in Archean composite grey gneiss complexes. J. Metamorph. Geol. 35, 181–195.
Wiseman, J.D.H., 1934. The central and south-West Highland epidorites: a study in progressive metamorphism. Q. J. Geol. Soc. Lond. 90, 354–417.
Yakymchuk, C., Clark, C., White, R.W., 2017. Phase relations, reaction sequences and petrochronology. Rev. Mineral. Geochem. 83, 13–53.
Yogi, M.T.A.G., 2016. Evolução estrutural e metamórfica do Antiforme da Anta Gorda, Faixa Ribeira Meridional: Testando a possível existência de um complexo de núcleo metamórfico extensional. Graduation Monograph. Institute of Geosciences - University of São Paulo, p. 44p.